Gabor Wavelets for Texture Edge Extraction

Juliang Shao and Wolfgang Förstner

Institut für Photogrammetrie, Universität Bonn,
Nußallee 15, D-53115 Bonn, Germany
Tel: 0049-228-732721, Fax: 0049-228-732712
E-mail: jls and wf@ipb.uni-bonn.de

Comm.III Symposium'94, WG/2

KEY WORDS: Gabor Wavelets, Texture Segmentation, Squared Texture Gradient, Natural Scene Analysis.

ABSTRACT:

Textures in images have a natural order, both in orientation and multiple narrow-band frequency, which requires to employ multichannel local spatial/frequency filtering and orientation selectivity, and to have a multiscale characteristic. Each channel covers one part of whole frequency domain, which indicates different information for the different texton. Gabor filter, as a near orthogonal wavelet used in this paper, has orientation selectivity, multiscale property, linear phase and good localization both in spatial and frequency domains, which are suitable for texture analysis. Gabor filters are employed for clustering the similarity of same type of textons. Gaussian filters are also used for detection of normal image edges. Then hybrid texture and nontexture gradient measurement is based on fusion of the difference of amplitude of the filter responses between Gabor and Gaussian filters at neighboring pixels by mainly using average squared gradient. Normalization, beased on the noise response and based on maximium response are computed.

1 Motivation

Texture analysis continues to be a bottleneck in Computer Vision, especially for natural scene interpretation. Texture is one of the basic characteristics of visible surfaces and of similar importance for perception as colour. It therefore plays a central role in a number of applications such as remote sensing, environment monitoring, medical image processing and quality assurance.
There are a number of tasks which are either much more complicated than their "untextured" counterparts or explicitely rely on the existence of texture.

- Segmentation and feature extraction aim at a (more or less) unsupervised derivation of a symbolic image description where the features, points, edges and segments are used for further processing. This may e. g. be used to derive a crude 3D-description for symbolic image matching.
- Classification of images aims at a direct derivation of a class label which usually carries a meaning in an application context. Texture may be helpful e. g. in remote sensing for increasing the quality of multispectral classification.
- Shape recovery [Super and Bovik 1992], in contrast to the two previous tasks, requires texture or is at least much easier with textured surfaces as many matching algorithms, be it intensity or feature based, are likely to fail in textureless areas. On the other hand, texture gradient, i. e. the gradual change of texture density, gives a direct cue for orientation of the underlying surface.

The approaches to texture analysis may be roughly described as structural, statistical and filter based.

1. The structural approaches (cf. e. g. Fu 1982, Vorhees and Poggio 1987) assume texture elements to exist, which in a regular or irregular manner constitute the texture. Examples are wallpaper patterns, the structure of honeycomb or - more irregular - the skin pattern of crocodiles. The roots of this approach go back to the simple observation that texture in an image is caused by a truely three dimensional structure, consisting of parts which are evolved or generated by the same process parallel over time. This is in contrast to statistical and filter based approaches which implicitely assume the texture to be an irregular reflectance function on an otherwise smooth surface.
   The reason why this structural approach has not really succeeded in texture analysis is the practically unlimited combination of basic patterns which themselves may also vary to a large degree. Therefore the *generation* of such patterns may very well be successful, e. g. when using fractal type structures, which is useful in computer graphics. The inverse problem however, has not been shown to be solvable over a larger range of patterns.

2. Statistical approaches are based on the opposite line of thought: It is irrelevant *how* a texture is generated as long as its statistical properties which are observable in an image are sufficient to perform segmentation or classification. The number of texture descriptions which have been proposed is large [Ahuja and Rosenfeld 1981]. One may distinguish ad hoc descriptors as the variance, the entropy or other measures of the local neighbourhood of a pixel and model based descriptors which allow generation and analysis of texture such as co-occurance matrices [Haralick 1979, Elfadel and Picard 1994], autoregressive models or Hidden Markov Random Fields [Hassner M. 198081, Kervrann and Heitz 1993, Chen and Kundu 1994]. A common property of all statistical approaches is their

implicit relation to the grid structure of the image. This prevents scaling up and down the descriptors (e. g. AR-coefficients) and multi-image integration, e. g. during matching. Though the coefficients usually are not rotation invariants which may be necessary for classification, some rotation invariant texture descriptors have been developed [Kashyap and Lapsa 1984].

3. Filter based approaches also follow a phenomenological reasoning. They assume the image function to be locally describable by their amplitude spectra [Lonnestad 1992, Chen and Kundu 1994, Chang and Kuo 1992, Bigün and du Buf 1994, Lee and Yuille 1992, Dunn and Wakeley 1994, Manjunath and Chellappa 1993, Fogel and Sagi 1989, Ng and Kittler 1992, Malik and Perona 1990]. In spite of close theoretical connections to the statistical approaches, the filter based approaches seem to have some distinct properties.

   - They are biologically plausible, as physiological findings support the idea of a filter bank with filters which are orientation and scale sensitive.
   - They are continuous models which may be descretized for implementation. For linear geometric transform the filter responses are predictable, allowing to integrate several images.
   - They have experimentally shown to be generic in the sense that natural and artificial textures can successfully be analysed.

   In spite of the good results reported, there is no commonly accepted way to select the filter bank and to link the different channels.

The primary motivation for the approach described in this paper was the need to extend our feature extraction concept [Förstner 1994] so that not only colour images [Brügelmann and Förstner 1992], but also textured images can be handled. The basic idea is to locally represent the image structure by a 2×2 matrix containing the averaged spatial squared derivatives (SSD) from which the homogeneity, the isotropy and the orientation of the local, possibly vector-valued image function can easily be derived and used for detecting points, lines and segments. None of the known texture analysis procedures provided this local energy measure. As we have had good experience with the approach by [Malik and Perona 1990], we wanted to apply a filter based approach based on some kind of wavelet. However, in contrast to the scope of Malik and Perona, we are primarily interested in analysing natural scenes, particularly aerial images which allow to replace the nonlinearities in their approach, possibly loosing some texture discrimination power at artificial images.

2 Finding Texture Boundaries

Texture segmentation is performed in three steps.

1. Analysing the local Fourier spectrum by a filter bank leading to a multichannel representation a_k of the image.
2. Combining the channels to obtain a scalar or tensor valued image indicating the total response of the image.
3. Detecting texture edges by some scheme known from scalar image edge detection.

2.1 The Multichannel Representation

We use the well-established Gabor wavelets due to the favorable properties they have shown in texture segmentation. They are orientation and scale sensitive and are defined as filter pairs G_k^o and G_k^e being windowed cos and sin waves.

$$G_k^o = g(x,y;s_k) \cdot \cos[2\pi(U_k x + V_k y)] \quad (1)$$
$$G_k^e = g(x,y;s_k) \cdot \sin[2\pi(U_k x + V_k y)] \quad (2)$$

with

$$U_k = \cos\varphi_k / s_k \; ; \; V_k = \sin\varphi_k / s_k \quad (3)$$

or with the complex valued filter

$$G_k = G_k^e + jG_k^o = g(x,y;s_k) \cdot \exp[j2\pi(U_k x + V_k y)] . \quad (4)$$

The window function g is a Gaussian

$$g(x,y;s_k) = \frac{1}{2\pi s_k^2} \cdot \exp\left(- \frac{x^2+y^2}{2s_k} \right) . \quad (5)$$

Remark: One can also choose a nonisotropic window function in order to put more emphasis on scale *or* orientation sensitivity (cf. Yuille and Geiger 1990). In our experiments we restricted to isotropic windows. □

The Fourier spectrum $\hat{G}_k$ of the Gabor filter G_k is given by a shifted Gaussian

$$\begin{aligned} &\hat{G}_k(u,v) \\ &= 2\pi s_k^2 \cdot g(u,v;1/(2\pi s_k)) * \delta(u-U_k, v-V_k) \\ &= \exp\{-2\pi^2 s_k^2 [(u-U_k)^2 + (v-V_k)^2]\} . \end{aligned} \quad (6)$$

2 sets of Gabor filters (impusle response) are shown in Fig. 1, which show their orientation and scale selectivity and their spatial localization property. We now obtain the

Figure 1: shows 2 sets of Gabor filters (impusle response) with $s_k = 4\,[pel]$ and $s_k = 16\,[pel]$ and orientations 0^o and 45^o resp.

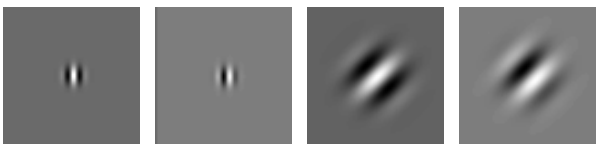

magnitude or amplitude of the filter response to the given image function $f(x,y)$

$$a_k(x,y) = \mid G_k * f \mid = \sqrt{G_k^o * f + G_k^e * f} . \quad (7)$$

Observe that (7) constitutes a nonlinear operation in the segmentation scheme. It is well-known (cf. Dunn and Wakeley 1994) that purely linear techniques cannot work; on the other hand using just the amplitude or amplitude squared and neglecting the phase of the complex Gabor response $G_k * f$ results in loss of discrimative power for certain textures as has been shown by [Malik and Perona 1990]. As mentioned in the introduction, we assume the loss caused by this first nonlinearity not to be relevant in natural scenes.

The vector-valued image $\{a_k(x,y)\}$ can be interpreted as a multispectral or colour image of which the edges have to be detected.

Example 1 Fig. 2 shows a test image with vertical sinwaves with wavelengths $\lambda = 2, 4, 8$ and 16[pel]. Fig. 1b, c, d, e show the amplitude responses of the Gabor wavelets with $\varphi = 0$ and $s_1 = 2, s_2 = 2\sqrt{2}, s_3 = 4$ and $s_4 = 4\sqrt{2}$. The responses are largest in Fig. 1c and e where the chosen scales s_k are tuned to the image pattern. At other scales s_k a non-zero response occurs. Thus a thresholding on the amplitude responses as means for texture segmentation will fail. However, summing up the gradient magnitudes of all amplitude responses yields the edge strength image shown in Fig. 1f from which the texture boundaries may be derived using non-maximum suppression. □

Figure 2: a) shows an artificial image consisting of 4 parts with scales 2, 4, 8 and 16 pixels. The amplitude of the Gabor responses with scales 2, 2.8, 4 and 5.6 are shown in b), c), d), e) respectively. f) shows the total gradient magnitude of the amplitude response.

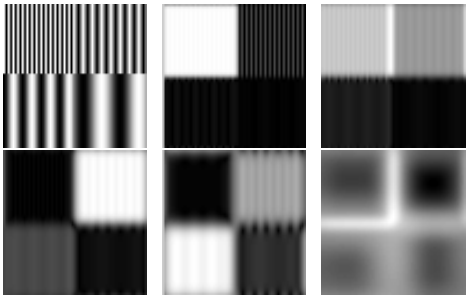

Example 2 A similar test pattern is shown in Fig. 3a together with the response of a Gabor wavelet tuned to the vertical pattern (3b). Observe that all type of boundaries occur: blurred step edges as well as positive and negative line edges. The phase shift between the two left patterns is revealed though the phase in the Gabor response has been eliminated. (This effect has been studied by Dunn et al. (1994). The gradient image is shown in Fig. 3c and d namely $\partial a_k/\partial x$ and $\partial a_k/\partial y$ indicating that searching for relative maxima here will also not give the desired edges. □

Figure 3: a) shows an artificial image with different oriented patterns. b) is the amplitude response which shows 3 types of edges. c) and d) are the gradient images of the amplitude response of b). Relative optima would lead to double edges between the two left textures.

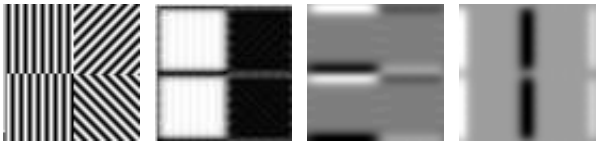

We therefore use our feature extraction scheme (cf. [Brügelmann and Förstner 1992] for detecting region boundaries, which is able to detect edge and line boundaries simultaneously.

2.2 Integrating the Channel Responses

The multispectral boundary detection scheme determines the average squared gradient

$$\overline{\Gamma a_k} = g_t * (\nabla_s a_k \cdot \nabla_s^T a_k) \tag{8}$$

of each channel k. Here

$$\nabla_s a_k = \nabla g_s * a_k = \left(\frac{\partial}{\partial x} g_s \; \frac{\partial}{\partial y} g_y\right)^T * a_k \tag{9}$$

denotes the gradient of a_k with smoothing kernel g_s. The width s of this kernel should be adapted to s_k of the Gabor filter, e. g. $s = s_k$ or $s = 2s_k$.
The integration of the squared gradient with the window g_t guarantees that edges and lines can be detected simultaneously. It strongly motivates this second nonlinearity. It can be shown that a line of width $2a$ is detected and not two edges if the integration scale is chosen to be larger than $1.5a$ (cf. Förstner 1994) suggesting $t_k = 2s$ (cf. Fig. 4).

Figure 4: a) shows a graph with a light line, a step edge, a dark line and a step edge. Using a small integration scale for the squared gradient results all edges, while using a large integration scale for the squared gradient (c) identifies the lines and the edges simultanously.

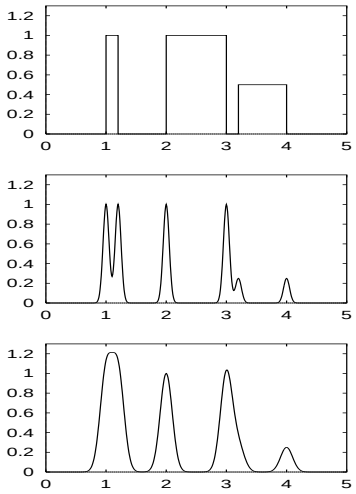

The edge strength h_k of each channel can be derived from

$$h_k = tr\overline{\Gamma a_k} = g_t * \parallel \nabla_s a_k \parallel^2 \; . \tag{10}$$

In order to integrate the different channels, we use a weighted mean

$$\overline{\Gamma a} = \sum_k \overline{\Gamma a_k} \cdot w_k \tag{11}$$

avoiding a further nonlinearity.
We investigated two choices of weights

a. The weight w_k is chosen according to the noise gradient response of the k-th Gabor filter

$$w_k = 1/\sigma_{h_k}^2 \; . \tag{12}$$

This implicitely assumes the *channels* to be *independent*; an assumption which can be only approximately

true, as Gabor wavelets do not form an orthogonal basis.
In our experiments we estimated the variance $\sigma^2_{h_k}$ by using a simulated noise image. The value $E(\sigma^2_{h_k}|g = n)$ may also be derived analytically.

b. The weight is chosen according to the range of a_k thus

$$w_k = 1/\max_{xy} h_k(x,y) \tag{13}$$

assuming that $h_k(x,y) = 0$.
This choice is motivated by the fact that weak texture edges in small scale channels may be buried in disturbances caused by improper scale tuning of larger filters (cf. the example of nonconstancy of the responses in Fig. 1c/e).

2.3 Locating Boundaries

From the total average squared gradient $\overline{\Gamma a}$ we can now derive three measures to be used for the boundary detection.

1. The edge strength

$$h = tr\overline{\Gamma a} \tag{14}$$

which should be locally optimum across the edge.

2. The orientation

$$\psi = \frac{1}{2}\arctan\frac{2(\overline{\Gamma a})_{12}}{(\overline{\Gamma a})_{11} - (\overline{\Gamma a})_{22}} \tag{15}$$

which is in the range $0 < \varphi < \pi$.

3. The isotropy measure

$$q = \frac{4\det(\Gamma a)}{tr(\Gamma a)} = 1 - \left(\frac{\lambda_1 - \lambda_2}{\lambda_1 + \lambda_2}\right)^2 \tag{16}$$

which is small for $\lambda_1 \gg \lambda_2$.

We only used the edge strength and the orientation for detecting texture edge pixels. The isotropy measure is shown in the graphs; its potential for detecting texture junctions has not been investigated yet.

3 Experiments

3.1 Implementation

We have realized the concept and tested it on various kinds of images.
The easiest implementation of the filters is using Fourier techniques. Though using the classical Fast Fourier Transform restricts the size of the images to powers of two, this is sufficient for testing the concept. The Gabor filters may be replaced by similar filters, e. g. using derivatives of the Gaussian (cf. Dunn and Wakeley 1994, Li and Shao 1994), which can efficiently be implemented in the spatial domain.

We used the above mentioned Gabor filters with regularity spaced orientation, and logarithmically spaced scales:

$$\varphi_l = l \cdot \Delta\varphi \quad , \quad l = 0, \ldots, L \tag{17}$$

$$s_m = s_o \cdot 2^{m \cdot \Delta s} \quad , \quad m = 0, \ldots, M \tag{18}$$

leading to a set $\{G_k\} = \{G(x, y; s_m, \varphi_l\}$, inducing a mapping $\{l, m\} \rightarrow \{k\}$.
In addition we use Gaussian's $g(x, y; s_m)$ for each selected scale s_m. Thus for each scale we have $m+1$ filters, a choice similar to [Malik and Perona 1990]. The Laplacian has not been found necessary in the examples we tested.

3.2 Choice of Filter Orientations and Scales

The automatic choice of the φ_l and s_m is an up to now unsolved problem. The reason simply lies in the definition of a texture which nearly always shows to be constructed of basic texture elements which themselves may also be textured (cf. the herringbone pattern analysed by Witkin 1983, who observed the recursive structure of this texture). It is therefore the task of the routine which calls the texture segmentation module to specify in which range it treats structure as texture. In our experiment we defined these values interactively. If not stated otherwise, we use a fixed number of orientation, namely $\varphi = i \cdot 30°, i = 0, \ldots, 5$ while we manually fix the range $[s_{\min}, s_{\max}]$ of scales which increase with a factor of $\sqrt{2}(\hat{=}\Delta s = \frac{1}{2})$.

3.3 Results from Artificial Data

We first present the results of the texture edge extraction for artificial data. Fig. 5, 6, and 7 are synthetic data which are supposed to demostrate the ability of the approach to handle texture of different orientation, phase and scale. In all case the homogeneity h, the isotropy q and an edge overlay is shown.

The homogeneity response h reveals the edges to be easily detectable, the strength however varying to a large degree. The isotropy q, which should be low (dark) at edges, confirms the subjective quality of the edges, being quite large at places where the edge has been detected.
The isotropy image q in Fig. 5c and Fig. 6c clearly shows the ansisotropic areas, i.e. the texture edge areas (dark). The light (isotropic) areas indicate either homogeneous texture or txeture corners.
The texture collages built from Brodatz-textures [Brodatz 1966] show the ability to discriminate the different textures. The textured areas are 32×32 pixels.
The homogeneity images h in Fig. 9a and c for the small collage Fig. 8 reveals clear differences between the two normalization scheme. The noise normalization yields smoother results, whereas the maximium normalization stronger reacts onto higher frequency changes, as to be expected.
The isotropy images q in Fig. 11a and c of the large collage Fig. 10 indicate the noise normalization to give a clear indication of the strength of the orientation of the edges. The isotropy image of the maximium normalization Fig. 11c is not very informative. This corresponds to theory, as the noise normalization has a statistical motivation (weight = 1/variance) which the maximium normalization is lacking.

Figure 5: shows an artificial image with differently oriented textures, the gradient magnitude,h, the isotropy q and the overlay of the extracted edges. Observe that q clearly indicates anisotropic areas (dark) and the phase shift between the left textures have been detected. Parameters: $\Delta\phi = 45^o$, $s_{min} = 2$, $s_{max} = 11.3$, $\Delta s = 1/2$.

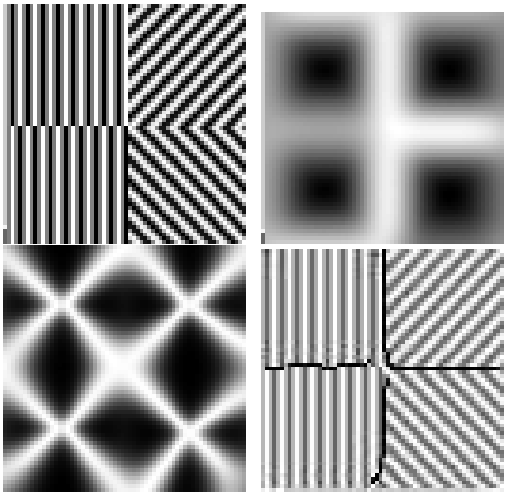

Figure 6: shows an artificial image with textures of different phase, the gradient magnitude h, the isotropy q and the overlay of the extracted edges. All 4 edges have been detected. Parameters: $\Delta\phi = 45^o$, $s_{min} = 2$, $s_{max} = 8$, $\Delta s = 1/2$.

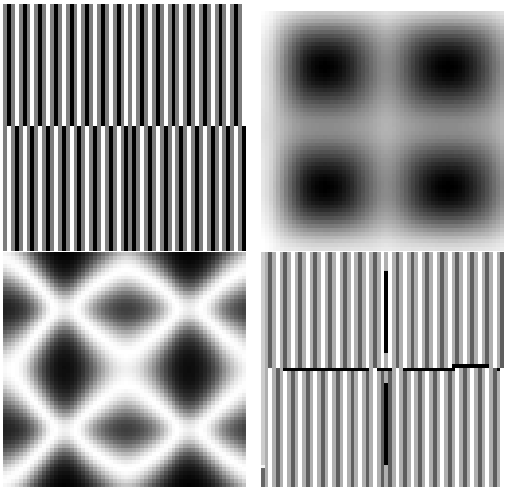

Figure 7: shows an artificial image with different scaled textures (cf. above), the gradient magnitude h and the overlay of the extracted edges. All 4 edges have been detected. Parameters: $\Delta\phi = 45^o$, $s_{min} = 2$, $s_{max} = 16$, $\Delta s = 1/2$.

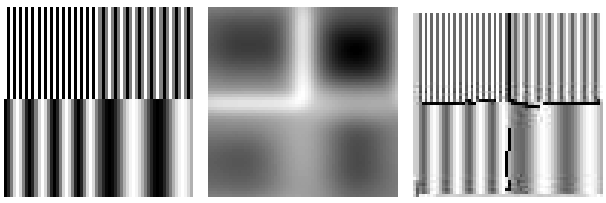

Figure 8: shows collage of four Brodatz-textures

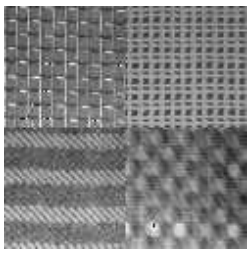

Figure 9: shows the gradient magnitude h and the overlay of the extracted edges for the previous figure. The textures are normalized to $\mu = 128$ [gr] and $\sigma = 32$ [gr]. a), b) and c) show the homogeneity h, the isotropy q and the edges for the noise normalization, d), e), and f) show the corresponding results for the maximium normalization. Parameters: $\Delta\phi = 30^o$, $s_{min} = 4$, $s_{max} = 45.2$, $\Delta s = 1/2$.

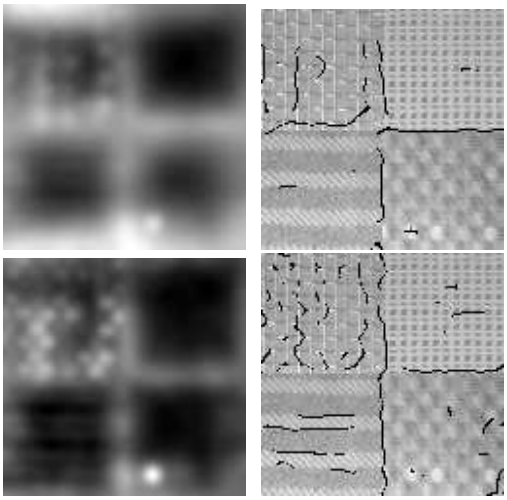

Fig. 12 shows a collage of two textures. Obviously the maximum normalization (13b) leads to a more closed boundary of the circular region than the noise normalization in Fig. 13a.

Figure 10: shows a collage of 16 Brodatz-textures

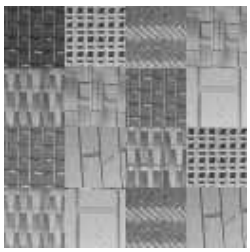

Fig. 14 shows the result of the texture edge extraction scheme on a textureless image. The results for the two normalization schemes are quite different: The noise normalization leads to blurred edges, suggesting the largest scale (here 2) to dominated whereas the maximium normalization tends to stress the smallest scale (here 1). In all cases no thresholding is performed.

Figure 11: shows isotropy q and the edges with noise- and maximium normalization for the previous figure.

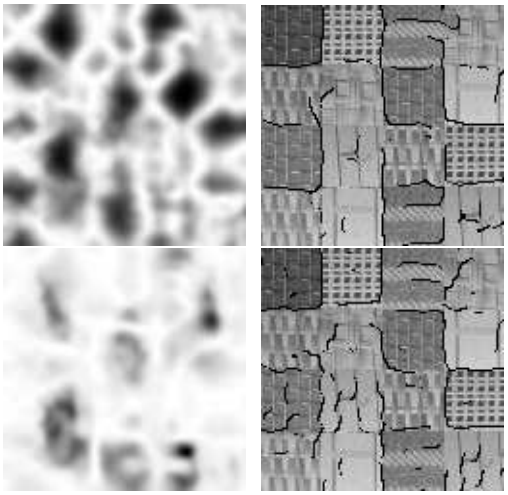

Figure 12: Collage of two Brodatz-textures

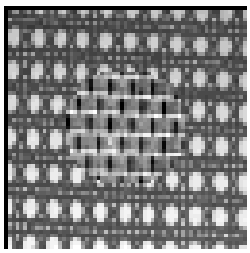

Figure 13: shows the extracted texture edges from the previous figure with noise normalization (a) and maximum normalization (b). Parameters: $\Delta\phi = 30^o$, $s_{min} = 2$, $s_{max} = 6.35$, $\Delta s = 1/3$.

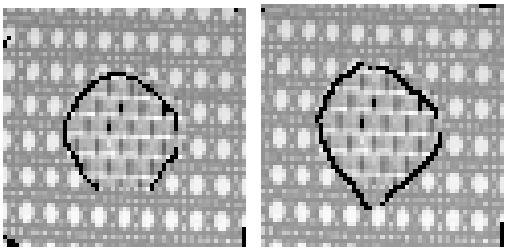

Figure 14: Toy image.

Figure 15: shows the extracted image edges from the previous figure with noise normalization (a) and maximum normalization (b). Parameters: $\Delta\phi = 30^o$, $s_{min} = 1$, $s_{max} = 2$, $\Delta s = 1/3$.

The examples clearly demostrate the approach to be able to extract edges of Brodatz-texture [Brodatz 1966]. the selection of scale however was tricky. The examples with natural images will more clearly show the difference between the two normalization schemes.

3.4 Results from Natural Scenes

Using section of aerial images [Gerster 1975] is to exploit the potential of the method for extracting texture edges which could be the basis for further segmentation. All examples are analysed using both weighting schemes. The scale parameters were interactively adapted, in all cases except the 4 directions φ we chosed.

In figure 17 both results capture the main texture edges. Noise normalization appears to yield smoother and less spurious boundaries. However the long texture boundary at the lower left part seems to adapt more to the real boundary with maximium normalization.

Figure 16: A section of an aerial image (Gerster 1975, p. 189)

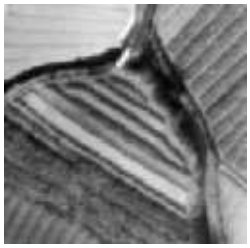

Also in figure 19 all texture boundaries have been detected. The horizontal edge in the upper left of the image is better recorded by the maximium normalization, where the boundaries of the small isles in the lower part of the image are better captured with noise normalization. Also here noise normalization yields the smoother edges.

Fig. 20 is a complicated case as it is questionable whether the structures should be treated as texture or rather should be analysed by grouping the fields. The image, however shows quite regular and nearly periodic structures, which suggests a filter based approach can be successful. Both normalizations (cf. Fig. 21) lead to quite good results. The noise normalization results fails to capture some short

Figure 17: shows the texture edges of the previous figure with noise- (a) and maximium (b) normalization, $\Delta\phi = 45^o$, $s_{min} = 2$, $s_{max} = 4$, $\Delta s = 1/3$.

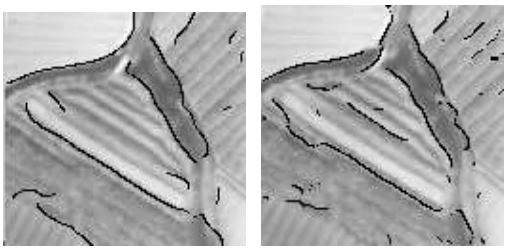

Figure 18: A section of an aerial image (Gerster 1975, p. 219)

Figure 19: shows texture edges of previous image with noise- (a) and maximium (b) normalization, $\Delta\phi = 45^o$, $s_{min} = 2$, $s_{max} = 4$, $\Delta s = 1/2$.

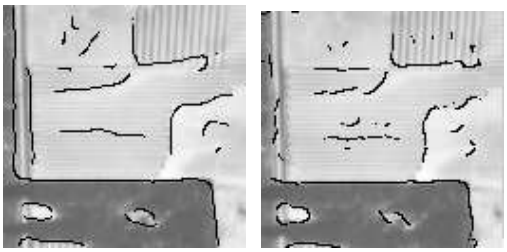

texture edges in the middle of the image. Both normalization do not find the bounday between the waved and the straight fields in the lower right of the image.

Figure 20: A section of an aerial image (Gerster 1975, p. 214)

Fig. 22 shows a field area with quite pronounced oriented textures. Both normalizations (Fig. 23) lead to quite convincing results, the noise normalization altogether appears to be a bit more close to reality.

Figure 21: shows texture edges of the previous figure with noise- (a) and maximium (b) normalization, $\Delta\phi = 45^o$, $s_{min} = 2$, $s_{max} = 11.2$, $\Delta s = 1/2$.

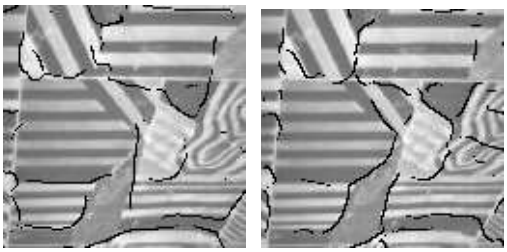

Figure 22: A section of an aerial image (Gerster 1975, p. 189)

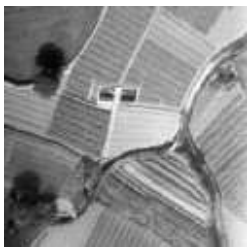

Figure 23: shows texture edges of the previous figure with noise- (a) and maximium (b) normalization, $\Delta\phi = 45^o$, $s_{min} = 2$, $s_{max} = 4$, $\Delta s = 1/3$.

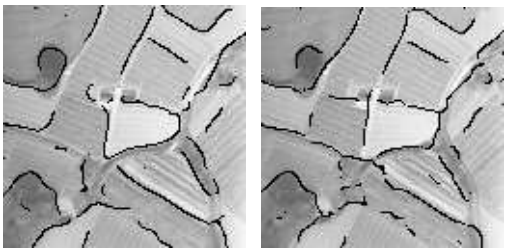

Observe that texture edges that are realized as small road are correctly extracted together with pure texture edges.

The last natural image in Fig. 24 is taken from a forest area which exhibits some regular and some irregular textures. Here only the noise normalization (Fig. 25) yields acceptable results, whereas the maximium normalization (Fig. 25) is not able to grasp even the clear boundary between the regular textures.

4 Conclusions

This paper presented a filter based approach to texture edge extraction using Gabor wavelets. The two nonlinearities within the procedure are squarings, one for obtaining the amplitude response of the filter, the other for deriving the squared gradient. The squared texture gradient has proven to be successful in detecting the different types of edges occuring in the amplitude images. The different channels have been integrated using two weighting

Figure 24: A section of an aerial image (Gerster 1975, p. 189)

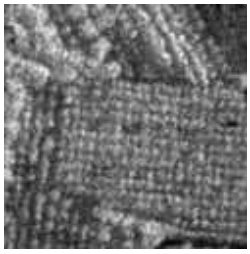

Figure 25: shows texture edges of the previous image with noise- (a) and maximium (b) normalization, $\Delta\phi = 45^o$, $s_{min} = 2$, $s_{max} = 11.2$, $\Delta s = 1/2$.

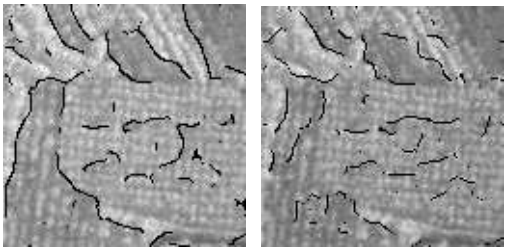

schemes: one based on the energy of the gradient response to a noise image, the other based on the maximum amplitude response. The noise normalization reacted more smoothly and more predictable onto texture edges while the maximum normalization scheme was able to grasp finer structures.
The approach was implemented and tested on a variety of real images and showed promising results.
The main problem left is the choice of the scale range and density, which in our experiments have been set interactivily. Also the use of the full information in the average squared texture gradient needs to be explored and is topic of our current research.

References

Ahuja, N.; Rosenfeld, A. (1981): Mosaic Models for Textures. *IEEE Trans. PAMI*, 3(1):1–10, 1981.

Bigün, J.; du Buf, J.M.H. (1994): N-folded Symmetries by Complex Moments in Gabor Space and Their Application to Unsupervised Texture Segmentation. *IEEE Trans. PAMI*, 16(1):80–87, 1994.

Brodatz, P. (1966): *Textures*. Dover Publications, Inc., 1966.

Brügelmann, R.; Förstner, W. (1992): Noise Estimation for Color Edge Extraction. In: W./Ruwiedel, Förstner (Ed.), *Robust Computer Vision-Quality of Vision algorothms*, pages 90–106, Bonn, 1992. Wichmann Verlag.

Chang, T.; Kuo, C. (1992): Texture Classification with Tree-Structures Wavelet Transform. In: *11th IAPR Intern. Conf. on PR*. IEEE Computer Soc. Press, 1992.

Chen, J.; Kundu, A. (1994): Rotation and Gray Scale Transform Invariant Texture Identification Using Wavelet Decomposition and Hidden Markov Model. *IEEE Trans. PAMI*, 16(2):208–214, 1994.

Dunn, D. Higgins, E.; Wakeley, J. (1994): Texture Segmentation Using 2-D Gabor Elementary Functions. *IEEE Trans. PAMI*, 16(2):130–149, 1994.

Elfadel, I.; Picard, R. (1994): Gibbs Random Field, Cooccurrences, and Texture Modeling. *IEEE Trans. PAMI*, 16(1):24–37, 1994.

Fogel, I.; Sagi, D. (1989): Gabor Filters as Texture Discriminator. *Biol. Cybern.*, 61:103–113, 1989.

Förstner, W. (1994): A Framework for Low Level Feature Extraction. In: Eklundh, Jan-Olof (Ed.), *Lecture Notes in Computer Science*, pages 381–394. Springer-Verlag Berlin Heidelberg, 1994.

Fu, K.S. (1982): *Syntactic Pattern Recognition and Applications*. Prentice-Hall, Inc., New Jersey, 1982.

Gerster, G. (1975): *Der Mensch Auf Seiner Erde*. Birkhäuser, 1975.

Haralick, R. M. (1979): Statistical and Structural Approaches to Texture. *Proc. IEEE*, 67:786–804, 1979.

Hassner M., Slansky J. (1980/81): The Use of Markov Random Fields as Models for Texture. In: A., Rosenfeld (Ed.), *Image Modeling*, pages 185–198. Academic Press, 1980/81.

Kashyap, R. L.; Lapsa, P. M. (1984): Synthesis and Estimation of Random Fields Using Long Correlation Models. *IEEE T-PAMI*, 6(2):800–809, 1984.

Kervrann, C.; Heitz, F. (1993): A Markov Random Field Model-based Approach to Unsupervised Texture Segmentation Using Local and Global Spatial Statistics. Technical report, IRISA, Capmus universitaire de Beaulieu, 1993.

Lee, T.; Mumford, D.; Yuille, A. (1992): Texture Segmentation by Minimizing Vector-Valued Energy Functionals: The Coupled-Membrance Model. In: Sandini, G. (Ed.), *Lecture Notes in Computer Science, Vol.588*, pages 165–173. Springer-Verlag Berlin Heidelberg, 1992.

Li, Deren; Shao, Juliang (1994): Wavelet Theory and Its Application in Image Edge Detection. *International Journal of Photogrammetry and Remote Sensing*, 49(3):4–11, 1994.

Lonnestad, T. (1992): A New Set of Texture feature Based on the Haar Transform. In: *11th IAPR Intern. Conf. on PR*, pages 676–679. IEEE COmputer Soc. Press, 1992.

Malik, J.; Perona, P. (1990): Preattentive Texture Discrimination with early Vision Machanisms. *J.Opt.Soc.Am.A.*, 7(5):923–932, 1990.

Manjunath, B.S.; Chellappa, R. (1993): A Unified Approach to Boundary Perception: Edges, Textures, and Illusory Contours. *IEEE Trans. Neural Networks*, 4(1):96–107, 1993.

Ng, I.; Tan, T.; Kittler, J. (1992): On Local Transform and Gabor Filter Representation of Texture. In: *11th IAPR Intern. Conf. on PR*. IEEE Comp. Soc. Press, 1992.

Super, B.J.; Bovik, A.C. (1992): Shape-from-Texture by Wavelet-Based Measurement of Local Spectral Moments. In: *Computer Vision '92 and Pattern Recognition*, pages 296–301, 1992.

Vorhees, H.; Poggio, T. (1987): Detecting Blobs as Textons in Natural Images. In: *Image Understanding Workshop, LA, Proceedings*, 1987.

Witkin, A. P. (1983): Scale Space Filtering. *IJCAI*, 1983.

Yuille, A.; Geiger, D. (1990): Stereo and Controlled Movement. *IJCV*, 4:141–152, 1990.